metals

MDPI

Article

Improvements in the Microstructure and Mechanical Properties of Aluminium Alloys Using Ultrasonic-Assisted Laser Welding

Ahmed Teyeb [1,*], João Silva [2], Jamil Kanfoud [1], Phil Carr [2], Tat-Hean Gan [1,*] and Wamadeva Balachandran [3]

[1] Brunel Innovation Centre, Brunel University London, Uxbridge UB8 3PH, UK; jamil.kanfoud@gmail.com
[2] Carr's Welding Technologies Ltd. (CWT), Kettering NN16 8PX, UK; john@carrswelding.co.uk (J.S.); pc@carrswelding.co.uk (P.C.)
[3] Department of Electronic and Electrical Engineering, Brunel University London, Uxbridge UB8 3PH, UK; wamadeva.balachandran@brunel.ac.uk
* Correspondence: ahmed.teyeb@brunel.ac.uk (A.T.); tat-hean.gan@brunel.ac.uk (T.-H.G.)

Abstract: Welding high-strength aluminium alloys is generally a delicate operation due to the degradation of mechanical properties in the thermally affected zone (TAZ) and the presence of porosities in the molten metal. Furthermore, aluminium alloys contain compounds that solidify before the rest of the base alloy, therefore acting as stress concentration points that lead to the phenomenon of hot cracking. This paper investigates the process of applying ultrasonic vibrations to the molten pool aluminium alloy AA6082 to improve both its microstructure and mechanical properties. We analysed conventional and ultrasonic-assisted laser welding processes to assess the sonication effect in the ultrasonic band 20–40 kHz. Destructive and nondestructive tests were used to compare ultrasonically processed samples to baseline samples. We achieved a 26% increase in the tensile and weld yield strengths of laser welds in the aluminium plates via the power ultrasonic irradiation of the welds under optimum ultrasonic variable values during welding. It is estimated that the ultrasound intensity in the weld melt, using a maximum power of 160 W from a pair of 28 kHz transducers, was 35.5 W/cm^2 as a spatial average and 142 W/cm^2 at the antinodes. Cavitation activity was significant and sometimes a main contributor to the achieved improvements in weld quality.

Keywords: laser welding; aluminium alloys; cracks; power ultrasonic; porosities

Citation: Teyeb, A.; Silva, J.; Kanfoud, J.; Carr, P.; Gan, T.-H.; Balachandran, W. Improvements in the Microstructure and Mechanical Properties of Aluminium Alloys Using Ultrasonic-Assisted Laser Welding. *Metals* **2022**, *12*, 1041. https://doi.org/10.3390/met12061041

Academic Editor: Antonio Riveiro

Received: 6 April 2022
Accepted: 13 June 2022
Published: 17 June 2022

1. Introduction

In laser beam welding, a pulsed laser beam is used to weld thin materials (with a thickness of less than 1 mm), whereas a continuous beam is used to obtain deep welds. It is, therefore, not necessary to chamfer the parts beforehand to widen access, as is commonly done in conventional welding. In addition, the use of a lasers improves the stability of the welding pool. This technique is often used to achieve significant production volumes in the automotive and aerospace industries. For instance, the introduction of disk and fibre lasers achieved laser power ceiling scales of up to 16 and 100 kW, respectively [1–4]. The main parameters arising in a conventional continuous laser welding process are laser power, laser collimation (vertical position of the beam waist relative to the workpiece), welding speed, the type of shielding and/or root gas, and the flow rate of the gas. These parameters affect different aspects of the weld; for instance, an increase in laser power will lead to an increase in the power density, whilst a variation in the welding speed will increase or decrease the interaction time (i.e., the time the laser beam impinges on the same area) [2]. First, laser welding depends on the light coupling effect between the laser beam and workpiece, making the technology extremely reliant on the reflectivity of the material to be welded. Secondly, the laser can provide a concentrated heat source. However, materials with high thermal conductivity tend to partially disperse the heat and affect the profile of the resulting weld, (i.e., shallow welds are formed). Materials such as aluminium and its alloys pose additional challenges, as they have a strong tendency to form cracks due

to several characteristics such as an extensive solidification range, a high thermal expansion coefficient, and large solidification shrinkage.

To mitigate the aforementioned challenges, a new technique called oscillating laser welding has recently been developed to improve the weldability of materials with novel high-performance mechanical properties. However, the materials are difficult to weld. The technique depends on the weaving of a narrow laser beam as it travels along the weld joint [4]. There are also new studies on vibration-assisted laser welding. During this method, weld objects are supported on a platform that is mechanically vibrated [5]. These studies demonstrate that grain refinement can be achieved during the solidification of moulds whilst using the mechanical vibration of the parts being welded. However, the solidification of cast moulds occurs at a much slower rate when compared to welding processes such as laser welding. The objective of recent studies has been to identify grain refinement at faster cooling rates [6]. Concerning the studies on vibration-assisted laser welding, most of them apply vibrations either in the infrasound band (<20 Hz) or the audible sound band (20 Hz to 20 kHz). It is possible to implement the former in an industrial environment, but it is very difficult to implement the latter due to its impact on the human auditory system and the need for additional personal protective equipment (PPE) [3]. Recent studies have shown that ultrasonic waves, i.e., waves of a frequency exceeding 20 kHz which are undetectable by the human ear, applied during welding operations, including laser melting, limit the growth of grain structures and lead to grain multiplication due to vibration impacts, shocks, or fluid flows acting as new nuclei [7–14]. This phenomenon is called ultrasonic grain refinement. Grain refinement is an essential tool used to improve material tensile and yield strengths, as implied by the well-known Hall–Petch equation, relating yield strength to mean grain size under assumed spherical grains, which is a good approximation for well-refined grain structures.

Welding high-strength aluminium alloys is generally a delicate operation due to the degradation of the mechanical properties in the thermally affected zone (TAZ) and the presence of porosities in the molten metal. In the TAZ, tensile and yield strengths can be reduced by up to 50% compared to nominal values, depending on the welded alloy and the process used [8]. Furthermore, during the laser welding of aluminium 6XXX, the formation and agglomeration of magnesium silicates (with a higher melting point than aluminium) provoke weld cracking during the solidification process. The aluminium alloy AA6082 (Al with 0.7–1.3% Si, 0.0–0.5% Fe, 0.0–0.1% Cu, 0.4–1.0% Mn, 0.6–1.2% Mg, and <0.15% of other elements) is highly crack-sensitive because it contains around 1% of magnesium silicide (Mg_2Si) [9]. To temper these effects, slower speeds can be used in conjunction with lower power, but this reduces one of laser welding's major advantages—its speed [15–17]. As a result, there are significant economic impacts (rejected welded materials and a loss of raw material, energy, and time) which prevent laser welding from being used in highly-sensitive applications such as those within aerospace [18–21].

The research reported in this paper focused on developing ultrasonic assistance for laser welding, which operates alongside the laser welding head. The aim was to produce high-power sonication waves to improve the weldability of crack-sensitive aluminium alloys. This is a relatively new research field with few publications (referenced above). Our work aimed to advance on this prior research by extensively investigating and quantifying improvements to a key, comprehensive set of weld structure properties achieved when using ultrasonic waves and benchmarked by conventional laser welded parts. This aim was accomplished by manufacturing and testing a set of samples which were welded using different parameters (laser power, welding speed, ultrasonic power, and ultrasonic frequency).

2. Experimental Procedure

The experimental set-up is shown in Figure 1. Two ultrasound transmission transducers, centrally located on the two parallel plates to be welded on opposite sides of and equidistant from the weld line, were used; i.e., the transducers did not move during our experiments relative to the plates, and both were always stationary in the laboratory frame

of reference. This arrangement was chosen in order to maximise the scope of our research as follows. As explained in detail in Section 3.7, this arrangement, which involved a set of nodes and antinodes along the plate-weld line interfaces, led to quasi-standing waves in the plate. Therefore, during a single pass of the laser along the weld line and using a single power output setting of the transducers, by taking samples for microstructural analysis at distributed locations along the weld line, one can collect data on the effect of ultrasound intensity on the weld microstructure over a continuous intensity range from the antinode level down to the nodal level. This is a fast and convenient method of collecting data to discover the optimum values of ultrasonic variables for weld improvement. When the optimum conditions are discovered, leading to prospects of a commercialised ultrasonically assisted laser welding system, the transducer(s) is located close to the weld line and moved along the weld line synchronously, with the laser spot positioned such that the spot experiences the same field intensity at all times.

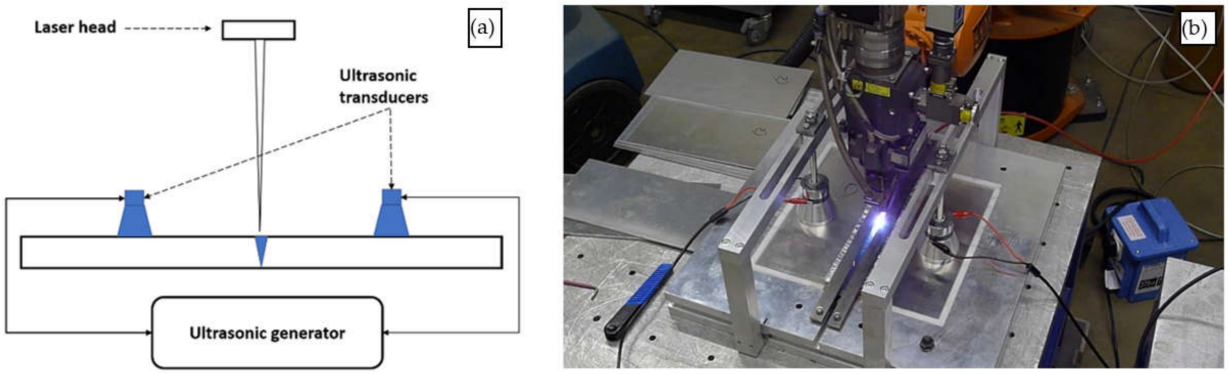

Figure 1. Experimental set-up for laser welding with ultrasound assistance: (**a**) schematics and (**b**) physical set-up.

The laser beam source used for the experiments was a high-power solid-state disk laser (TruDisk 6002) from Trumpf (Ditzingen, Germany), with a maximum power of 6 kW and a set wavelength of 1030 nm. The fibre diameter was 400 µm, coupled to a Kuka Kr16 6-axis robotic arm. The laser optic was a D70 Laser head also from Trumpf (Ditzingen, Germany), with a 200 mm focal length of collimation and a lens with a focal length of 200 mm. The selected laser collimation was −2 mm; i.e., the laser beam waist was focused 2 mm below the surface of the plates to be welded. The laser parameters were modified directly on the laser source console whilst the Kuka robotic arm controlled the linear welding speed. As shown in Figure 1b, to protect the bulk of the parent metal plates from excessive heating, two metal strips were rested on top of the plates on either side of the weld line and laser spot.

In the present study, a bespoke ultrasonic generator was developed to drive commercially available, high-power ultrasonic transducers (Piezoelectric Ultrasonic Cleaning Transducer (PZT-4) of Beijing Ultrasonic Co. Ltd., Beijing, China, with a diameter of approximately 7.5 cm at selected processing parameters, i.e., power and frequency. The system can output sine, square, sweep, barker code, and custom imported wave types. The material chosen for the welding trials was AA6082-T651 in the shape of flat plates. The plates all had a length and a width equal to 300 and 150 mm, respectively. However, their thicknesses varied throughout the trials, as one objective of this study was to identify the effect of the ultrasonic waves on different material thicknesses. The chosen thicknesses were 1.5, 2, and 4 mm. Every set of trials had constant laser settings to minimise the effect of the laser parameters on the experiments. The tests were segregated by the thickness of the aluminium plates being welded, and each plate received designated laser settings.

2.1. Laser Welding Set-Up

The laser power was kept constant for each plate thickness; for the 1.5 and 2 mm plates, 2 kW was used, and 3 kW was used for the 4 mm plates. The main reason for this variance was to assure that a full penetration weld occurred during the trials.

Two values of laser travel speed were used, 0.025 and 0.040 m/sec, for every set of trials. This weld speed range was deemed to be within the no-hot-cracking window specified [9], and it is the range generally used when autogenously welding 6082-grade aluminium. The beam waist position was kept fixed for every trial at −2 mm. The chosen shielding gas was argon (99.99%), with a flow rate of 14 L/min.

Throughout the experiments, 28 kHz-100 W (68 mm diameter) and 40 kHz-60 W (48 mm diameter) transducers (a pair of each) were used at 50% and 80% of the maximum power.

2.2. Sample Preparation

Surface Quality: Using an Optimax Evo Cam II, several pictures were taken and compared with the top surface of the trial plates.

Weld Geometry: To evaluate the weld geometry, every trial plate was sectioned (transversal cut) at the same locations (75, 150, and 225 mm) using an industrial metal saw (MetCut 300) and hot-mounted using a black epoxy resin and an automatic mounting press (OmegaPress EVO). Subsequently, the samples were polished on a metallurgical polisher (OmegaPol Twin 200 mm) using different wet/dry sandpapers (grit sizes: 240, 320, 400, 600, 800, 1000, and 1200) and water-cooled. The colouring of the weld zone was achieved by immersion in Keller's reagent (190 mL of H_2O, 5 mL of HNO_3, 3 mL of HCL, and 2 mL of HF) for 5 min. Finally, the macroanalyses were obtained by reflected light microscopy using a video microscope (Optimax Live Camera).

Grain Structure: Keller's reagent, used to evaluate the weld geometry, is not ideal for grain analysis. With this in mind, the samples were repolished using different wet/dry sandpapers (1200, 2000, and 2500 grit) and finalised with a diamond suspension emulsion (particle size of 3 µm). The chosen etching method was Barker's reagent with electrolytically anodised samples (25 V and 0.1 A for 60 s) examined under polarised light. Finally, the microanalyses were obtained by reflected light microscopy using a video microscope (Optimax Live Camera).

Scanning electron microscopy was used to produce images by scanning the surface of a sample with a focused beam of electrons. The addition of an EDX system (an energy dispersive X-ray analysis system) coupled with the SEM allowed for the identification of the elemental composition of the samples (and inclusions). The machine used was a Zeiss Supra 35VP with EDS, at the Experimental Techniques Centre (ETC) of Brunel University, London, with magnifications of up to 10,000×. The software used was the TEAM™ EDS Analysis System.

Tensile Strength: Transverse weld specimens were prepared following BS EN ISO 4136 and sent to an independent UKAS accredited laboratory for analysis.

3. Results and Discussion

3.1. Plasma Cloud

The first noticeable improvement when the ultrasonic wave was used during laser welding was the visible reduction of the plasma cloud, as shown in Figure 2. This was noted in every ultrasonic-assisted trial compared to the baseline (laser welding without ultrasound). The ultrasonic waves helped to balance and stabilise the keyhole, which minimises the pressure build-up and stops material ejections. The plasma cloud is then reduced due to lower pressure build-up.

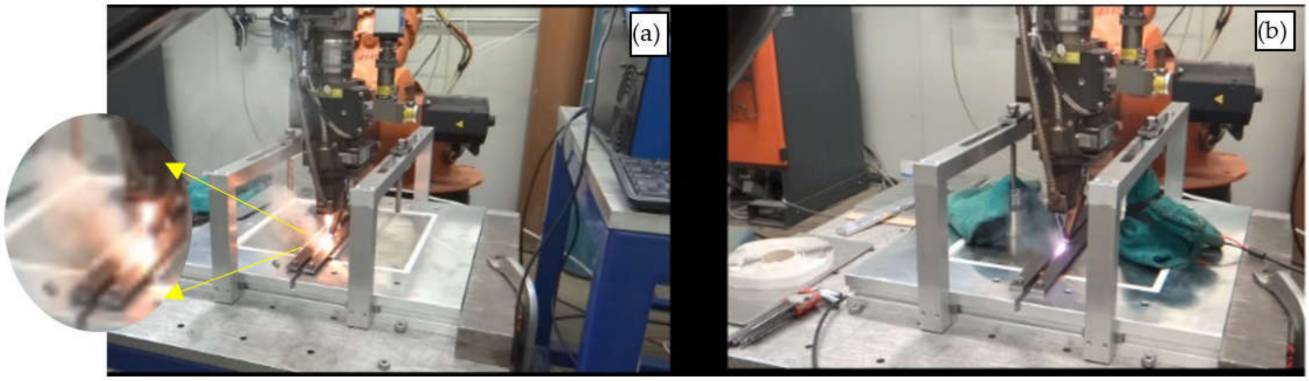

Figure 2. Plasma cloud captured by the monitoring camera during the welding process: (**a**) with no ultrasound used and (**b**) when ultrasound was used.

3.2. Aspect Ratio

The effect of the ultrasonic waves led to different weld aspect ratios (i.e., the ratio of surface weld width to root), as summarised in the various images captured in Figure 3, and reported in Table 1. It is worth noting that, with the thinner plates (1.5 and 2 mm), the use of the 40 kHz transducers led to smaller aspect ratios, whilst on thicker plates (4 mm), the converse was observed. The wave penetration decreases along the axis of the plate thickness with increasing frequency because both wave absorption and scattering in the weld melt increase with frequency. Thus, to achieve complete coverage of the weld joint, the frequency must be reduced commensurately with increasing plate thickness.

Based on the observation of the microscopy images shown in Figure 3a–f, at a plate thickness of 1.5 mm, the straightness of the weld profiles improved; i.e., the aspect ratio was smaller when ultrasound was used at a given laser power and welding speed. The weld profile became 43% straighter when the 40 kHz transducer was used. With the plates that were 4 mm thick or thinner (Figure 3g–k), the use of ultrasound at 28 kHz decreased the aspect ratio even further by 62%. However, 40 kHz ultrasound led to a reduction of only 14% when compared to the baseline. Compared with the thinner plates, the 28 kHz transducer achieved smaller aspect ratios on the thicker plates.

It is important to note that the effect of ultrasonic assistance was higher with the thinner plates (1.5 and 2 mm). We used two fixed transducers, and the wave was stronger at the parts closest to the transducers and tended to be attenuated in the parts of the weld joint that were farther from the transducers. Whilst there were still noticeable improvements in weldability and surface quality, the weld profile (Keller's etchant) in the baseline trials (without ultrasound, see Figure 3a,d,g,j) was nearly identical to the ultrasonic-assisted laser welding. Despite a noticeable benefit derived from the use of ultrasound assistance, it was also noted that, to be more effective, the ultrasonic contribution should be modulated to the size of the workpiece to be welded. For instance, whilst 40 kHz ultrasound improved weld profiles on the thinner plates (1.5–2 mm), the opposite was observed on thicker plates (4 mm), where the use of 28 kHz ultrasound generated more minor variations in the surface and root width.

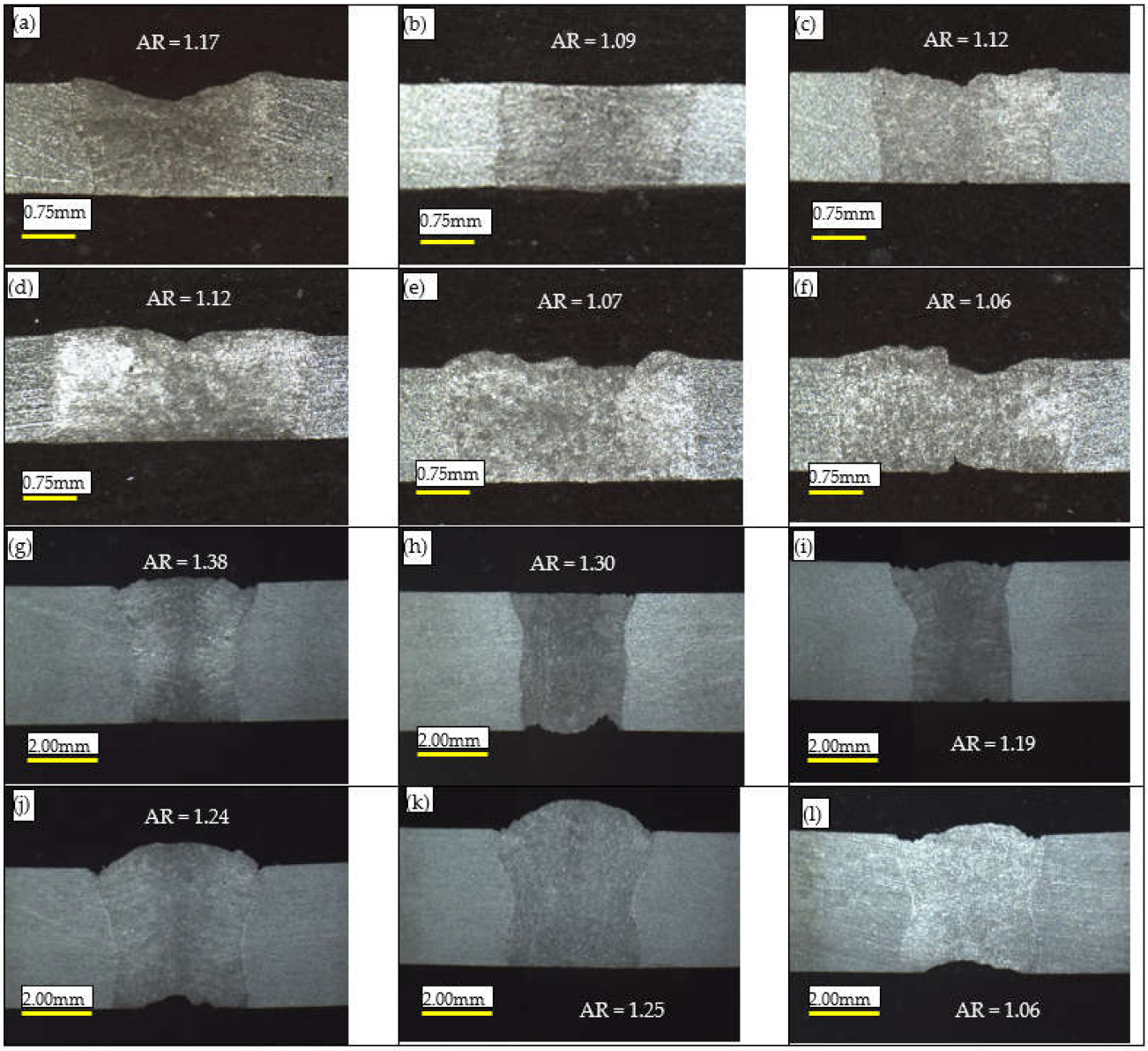

Figure 3. Aspect ratios of welds achieved at different configurations (T: plate thickness, WS: welding speed): (**a**–**c**) T = 1.5 mm, WS = 40 mm/s; (**a**) no ultrasound; (**b**) 2 × 40 kHz-30 W transducers; (**c**) 2 × 40 kHz-50 W transducers. (**d**–**f**) T = 1.5 mm, WS = 25 m/s; (**d**) no ultrasound; (**e**) 2 × 40 kHz-30 W transducers; (**f**) 2 × 40 kHz-50 W transducers. (**g**–**i**): T = 4 mm, WS = 40 mm/s; (**g**) no ultrasound; (**h**) 2 × 40 kHz-50 W transducers; (**i**) 2 × 28 kHz-80 W transducers. (**j**–**l**) T = 4 mm, WS = 25 mm/s; (**j**) no ultrasound; (**k**) 2 × 40 kHz-50 W transducers; (**l**) 2 × 28 kHz-80 W transducers.

Table 1. Average difference between weld width and root width in mm with different set-ups.

Thickness	Baseline	28 kHz	40 kHz
1.5 mm	0.375	0.340	0.215
4 mm	0.965	0.365	0.830

3.3. Surface Quality

Examination of the surface quality of the welds confirmed the overall effectiveness of using ultrasonic power during the welding process. In Figure 4a,b, concerning baseline samples, microcracks that are likely to be a crack initiation zone can be easily identified

and spotted across the weld line. However, in Figure 4c,d, when ultrasound was used, the weld line completely disappeared, and an improvement in grain arrangement was noted.

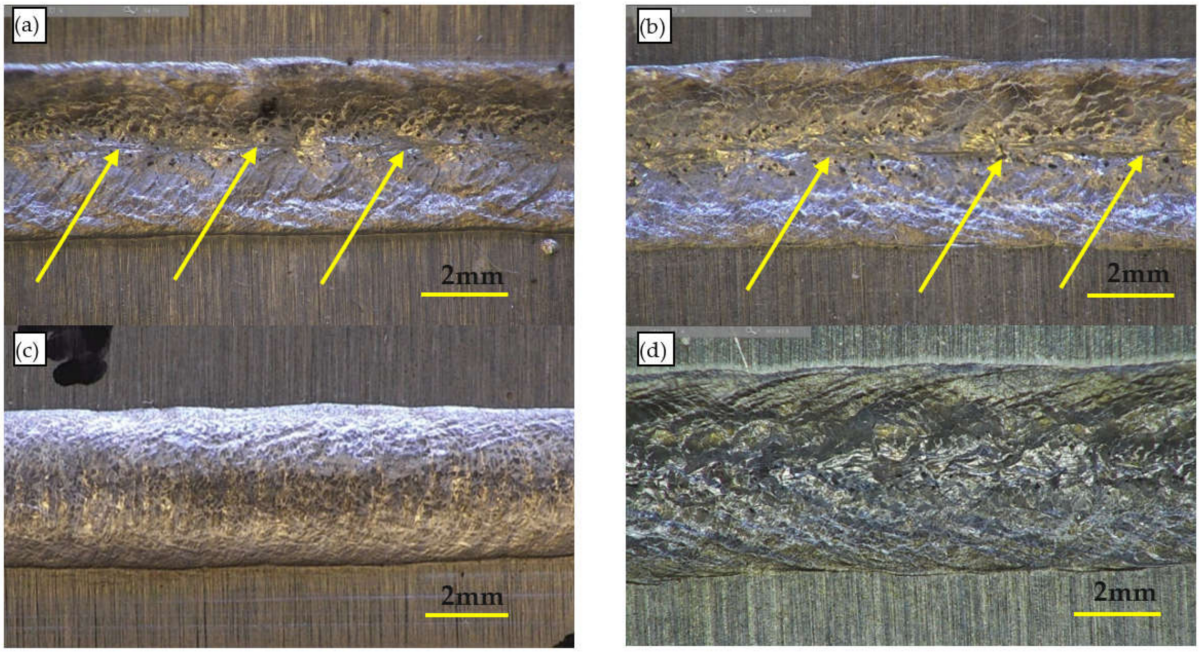

Figure 4. Examination of the surface of the welds achieved without ultrasound at (**a**) 25 mm/s and (**b**) 40 mm/s and with ultrasound at (**c**) 28 kHz, 80 W, and 25 mm/s and (**d**) 40 kHz, 50 W, and 40 mm/s. The arrows point to the central line of the weld (noticeable only in nonultrasound samples (**a**,**b**)).

3.4. Micro-Structure Analysis

As shown in Figure 5a, no agglomerations were noted in the SEM analysis without sonication. Linear intermetallic formations can be seen over the entire sample. These are more likely to act as crack initiators when compared to the spherical nature of the intermetallic structures seen in the second sample shown in Figure 5b, where ultrasound was used. In that case, no agglomerations were observed throughout the SEM analysis, and intermetallic formations were smaller and appeared mostly in the shape of spheres.

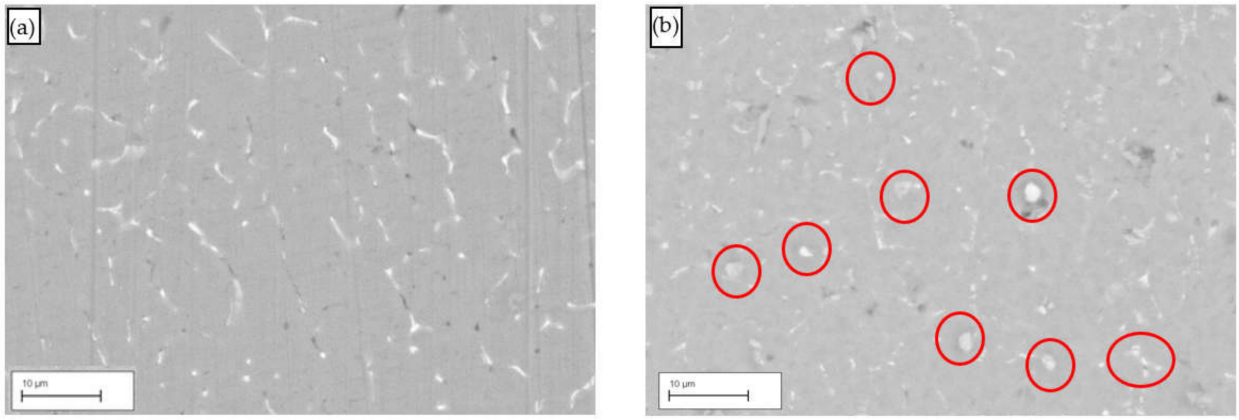

Figure 5. SEM analysis of cross sections of welds (2 mm thick plates) achieved at 25 mm/s (**a**) without ultrasound and (**b**) with ultrasound at 40 kHz and 50 W (spherical nature of the intermetallic structures).

3.5. Grain Structure Analysis

The reflected light microscopy images of the samples produced with and without ultrasound are shown in Figure 6. Without ultrasound, dendritic growth is evident (i.e., a tree-like structure in Figure 6a) in several locations throughout the weld zone. An unevenly distributed grain structure can also be seen. When ultrasound was used (Figure 6b), no agglomerations were noted in the analysis. The grain structure appears evenly distributed. However, a higher concentration of grains can be seen in the zones where different solidification fronts meet.

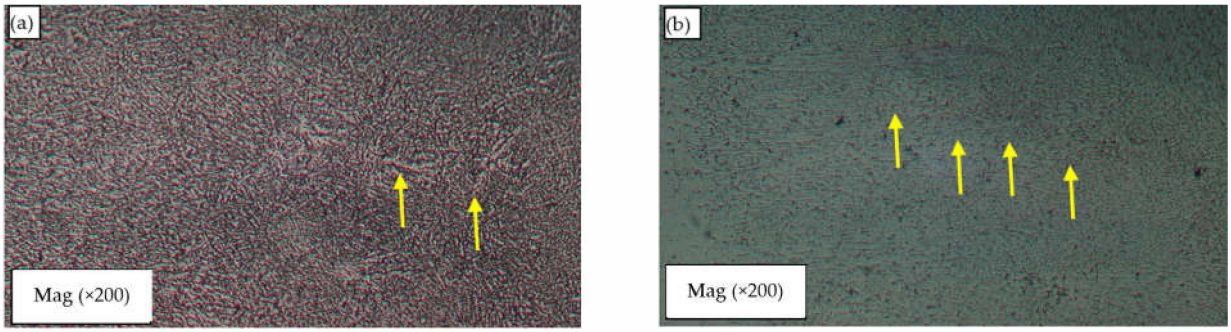

Figure 6. Reflected light microscopy images (×200 magnification) of cross sections of welds (2 mm thick plates) achieved at 40 mm/s (**a**) without ultrasound (arrows indicating some dendrites) and (**b**) with ultrasound at 40 kHz and 50 W (arrows indicating some solidification fronts).

Without ultrasound, the number of grains per area appeared higher than that obtained with ultrasound. It was also possible to identify dendritic growths and an increased concentration of grains around these growths. In the trials with ultrasound, the grain structure appeared to be more homogenised and evenly distributed, and it was also possible to identify a boundary with different grain sizes (solidification front).

3.6. Tensile Tests

Tensile tests were carried out on 1.5 mm thick samples, only with smaller aspect ratios, and superior surface quality was achieved at this thickness. The samples were prepared at laser scan speeds of 25 and 40 mm/s. Accordingly, the results were segregated into two groups. The sonication was conducted with transducers of 28 kHz (at 50 W and 80 W) and 40 kHz (at 30 W and 50 W). Baseline trials without sonication were also subjected to tensile tests to assess the sonication effect when compared to conventional laser beam welding.

Figure 7 shows the load vs. extension and the ultimate tensile strength of the welds at 40 mm/s, and Figure 8 shows the test results at 25 mm/s.

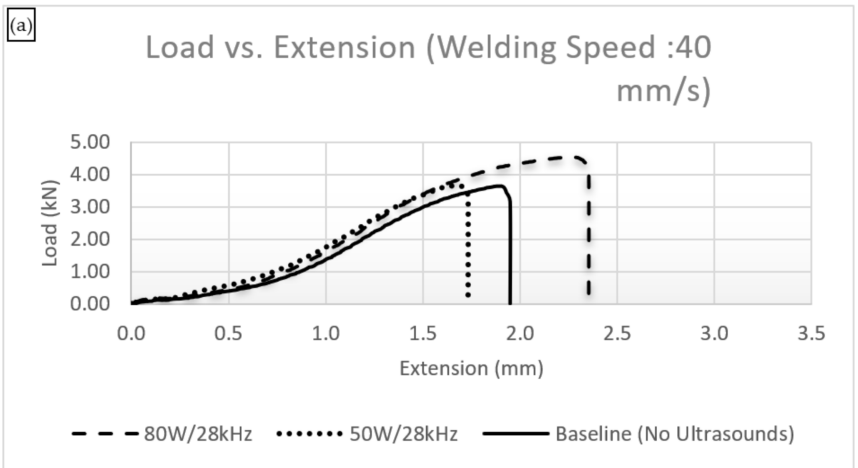

Figure 7. *Cont.*

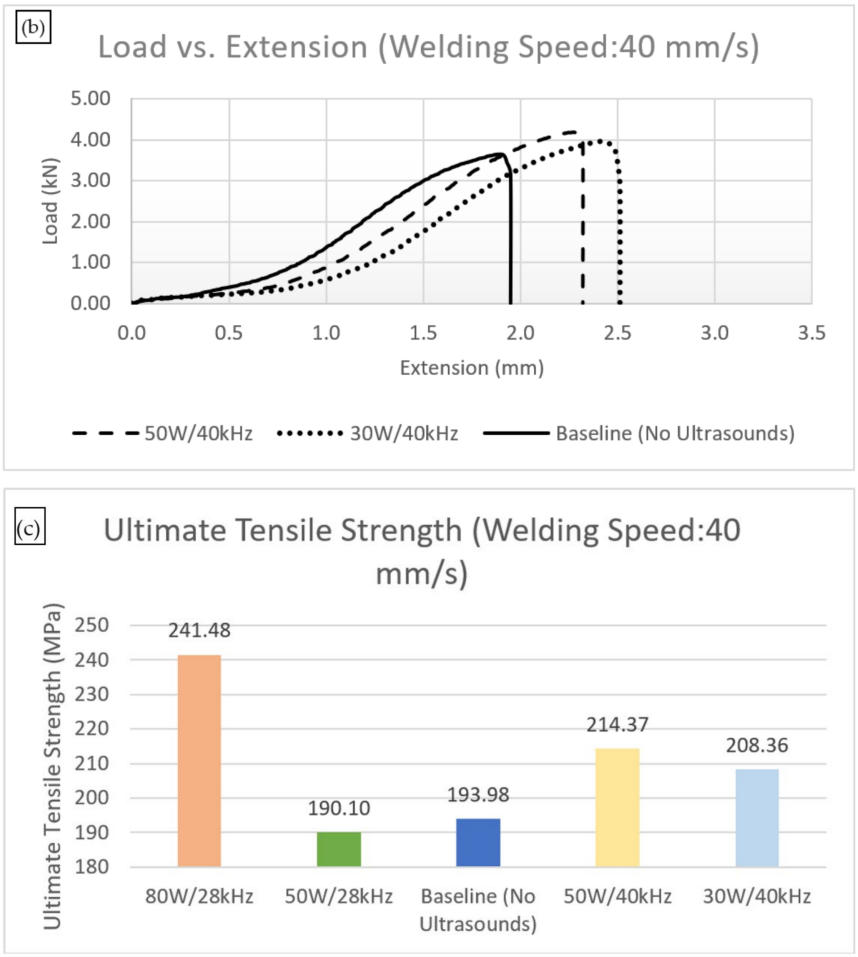

Figure 7. Load vs. extension (**a**) at 28 kHz, 40 mm/s, and (**b**) at 40 kHz, 40 mm/s. (**c**) Ultimate tensile strength at 40 mm/s.

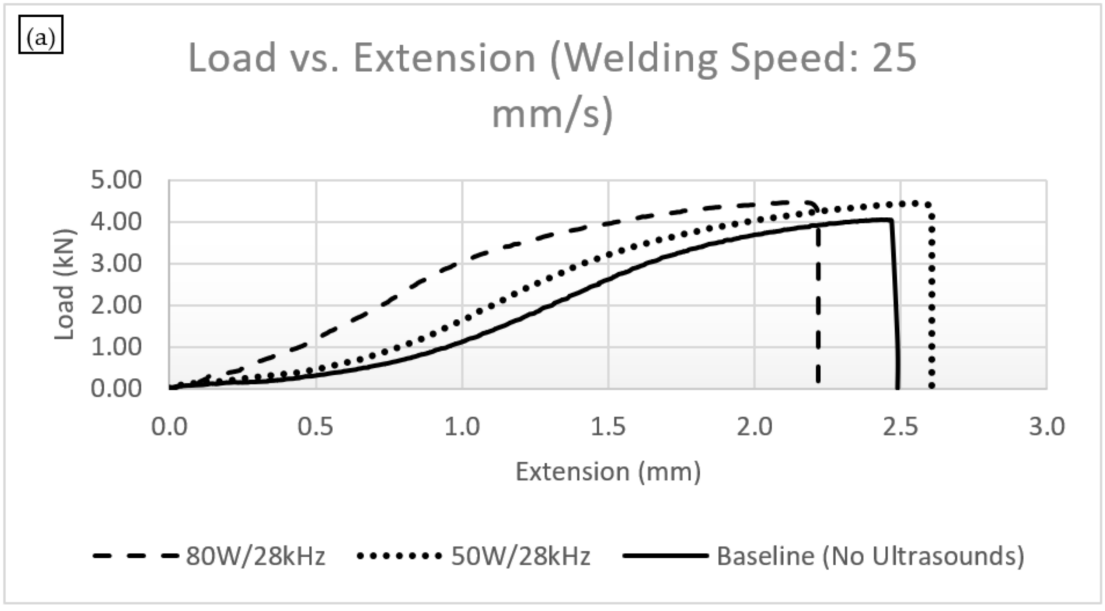

Figure 8. *Cont*.

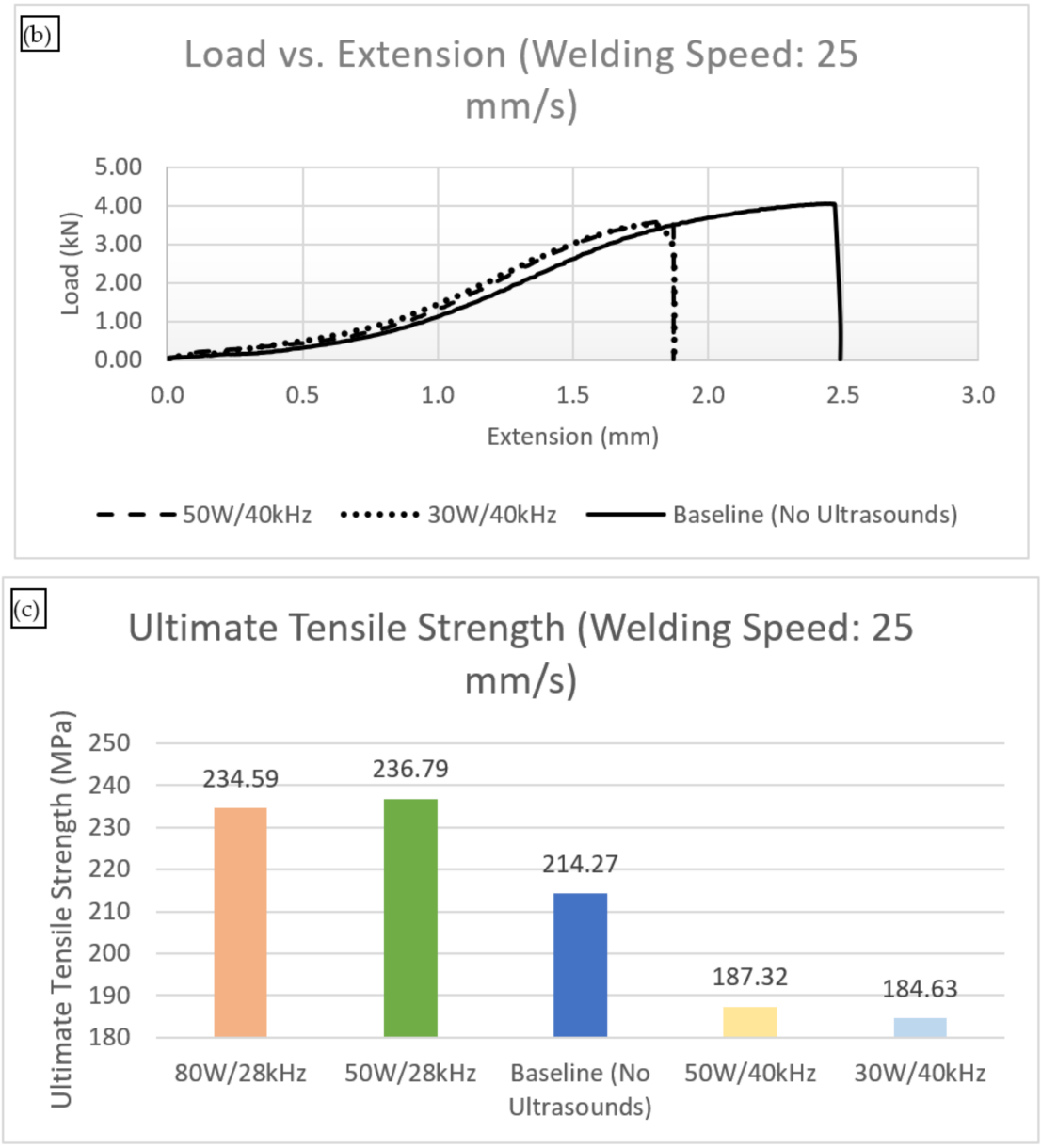

Figure 8. Load vs. extension (**a**) 28 kHz, 25 mm/s, (**b**) 40 kHz, 25 mm/s, and (**c**) ultimate tensile strength at 25 mm/s.

It can also be seen in Figure 8 that, when ultrasound was used, we achieved an average increase of 10% in both ultimate tensile strength and the load required for failure. The maximum values were achieved at a frequency of 28 kHz. An interpretation of this result is suggested in Section 3.7, where we estimate the ultrasound intensity in the melt in relation to cavitation thresholds.

Despite the inevitable decrease in local strength due to the fusion process, in a trial with a power of 80 W, a frequency of 28 kHz, and a welding speed of 25 mm/s, the ultimate tensile strength was 25% higher than the baseline trial. This increase could be explained by the homogenisation of the molten pool and the consequent reduction in crack initiation zones (e.g., dendritic growths).

3.7. Discussion of the Mechanisms Involved in the Weldment Changes Induced by Ultrasound

Here, we review the possible ultrasonic mechanisms that may have been the cause of the improvements we observed in the structure of the laser welds formed in the presence of power ultrasound.

The strongest mechanism of ultrasonic action on fluid phase materials, especially grain refinement, is cavitation. In cavitation, enormous local forces, large enough to rupture chemical bonds and raise local temperatures up to 10,000 K, acting on solid particulates in a melt, are generated by collapsing bubbles. These forces are many orders of magnitude greater than the secondary ultrasound radiation forces between the nearest neighbouring melt particulates, generated by ultrasound scattered by the particulates and the primary ultrasound radiation beam forces acting directly on the melt particulates. These forces (also called Bjerknes forces) combine to help keep the particles apart and hence reduce the tendency towards agglomeration and porosity formation and promote the spatial uniformity of particle distribution; however, the process is prolonged due to the low level of these forces. Thus, they can be effective in metal melts that exist for a long time, e.g., in a furnace or when continuously heated by a laser. However, it is unlikely that they would be very effective in laser spot welding, where the molten period at any point along the weld line lasts for only around a second.

Only cavitation forces are strong enough to break up the large and agglomerated grains in melts into smaller structures, and such structures will usually appear accidentally during melt cooling. The times for bubble growth and subsequent collapse to release cavitation forces are ~1 ms and 150 μs, respectively, so these forces can be effective in weld melts produced by rapidly moving laser spots.

The cavitation threshold intensity for aluminium melts has been published in the literature as 100 W/cm^2 [17]. It was not possible to determine whether cavitation forces were present in our experiments via the direct visual observation of bubbles in the melt because the melt was opaque, and our visual examination of the weld surfaces showed no surface emergence of bubbles. Thus, the likelihood of cavitation presence requires a calculation of the ultrasound power entering the melt. In order to accurately determine whether or not cavitation could have been present, we would need to compute the ultrasonic field in the entire weld-plate structure. This field is complex, consisting of quasi-standing waves, and requires modelling for an accurate prediction of the intensity levels achieved in the weld melt for a given transducer output power, which we will perform in future work. However, a rough calculation of this intensity can be readily performed as follows.

Knowing that the compressional wave velocity in the aluminium plates is 6000 m/s [18], the wavelengths would be 21.4 cm and 15 cm at 28 and 40 kHz, respectively, which are larger than the cross section of the transducer interface. Therefore, the radiation from the transducers will be omnidirectional. The absorption in the plates outside the melt region will be negligible at such long wavelengths and low frequencies. Therefore, multiple reflections at the plate boundaries, combined with negligible absorption losses, ensure that most of the power leaving the transducers will cross the plate–weld melt interfaces, although there will be some losses due to the leakage into the surrounding experimental apparatus and even directly into the air. For simplicity, we will neglect the latter.

Thus, with the highest power used, 80% of the power of two 100 W transducers (160 W) will cross the weld line–plate interface. The area of the interface for the 1.5 mm thick and 30 cm long plates used for the tensile testing experiments was, therefore, 4.5 cm^2. In addition, the spatially averaged intensity was 160 W/4.5 cm^2 = 35.5 W/cm^2. Assuming a compressional wave velocity in the weld melt of 2000 m/s, the wavelength in the melt at 28 kHz was around 7 cm. Therefore, a set of around 6 antinodes and nodes would have been present along the 30 cm long weld line. At the antinodes, the wave intensity would be four times the average, i.e., 142 W/cm^2. Therefore, we conclude that the cavitation threshold was well exceeded at the antinodes and cavitation, thus making a significant or even dominant contribution to the ultrasonically improved ultimate tensile strength of the welds. We noted in Section 3.6 that the same improvement in ultimate tensile strength arose

when transducer power outputs were reduced from 80 W to 50 W. For two 50 W transducers, the intensity in the melt at the antinodes would have been 89 W/cm^2, according to our calculation in Section 3.7, which is very close to the published cavitation threshold of 100 W/cm^2 referenced earlier in this subsection. One simple possible explanation is that far exceeding the threshold does not significantly increase bubble growth and collapse activity.

In a future publication, we will apply the Hall–Petch equation to our yield strength and grain size data to confirm that yield strength improvement stems from ultrasonic grain refinement in our welding process.

3.8. Other Possible Effects of Ultrasound on Weld Melts

High-power ultrasonic waves are known to disperse alloying compounds, such as magnesium silicide, towards the weld boundary, thereby minimising the risk of cooling residual stresses, leading to the hot cracking phenomenon. Additionally, ultrasonic waves improve weld quality by reducing overall imperfections due to porosities and oxide formation. It is possible that high-power ultrasound forces could mitigate the negative effect of Marangoni flow. Marangoni forces arise from surface tension gradients and can adversely affect weld strength by introducing spatial variations in the microstructure. Ultrasound could agitate the flow of the liquid melt at different solidification phases. This would result in an even heat distribution.

4. Conclusions

Our mechanical analysis and tensile testing identified the parameters that led to an average increase in the ultimate tensile strength of 10%. The best trial of the study improved the ultimate tensile strength by 25% compared to the baseline, where no ultrasound was used. The weld profile became straighter when ultrasound was used, with the difference between weld width and root width being reduced by 14–62%, depending on the set of parameters used.

The use of high-intensity ultrasound effectively disrupted the epitaxial growth of the dendrites, refined the grain structure, reduced the plasma cloud, and transformed the shape of the intermetallic compounds from linear to spherical. It also improved weld stabilisation and decreased the spatter levels, which are critical to weld quality and weld strength.

The resistance to crack propagation–crack initiation due to grain refinement and disruption of the epitaxial growth of dendrites is linked to the increase in ultimate tensile strength and the load required for failure. A noticeable improvement was observed during the trials using high-intensity ultrasound.

Future work should seek to broaden the range of values of the sonication parameters (frequency and power) and the topological ranges of different test pieces (thickness, shape, curvature, etc.) in order to determine the optimum values, i.e., those that maximise weld improvement for a prescribed cost/energy expenditure. We will also conduct a more quantitative analysis of the present data using the Hall–Petch equation, relating equiaxed grain size to yield strength and related models. Finally, the radiation field in the plates and across the weld melt–plate interfaces will be modelled to confirm that cavitation was a significant contributor to weld quality improvement in the experiments reported here. Such a model will reveal the locations of the nodes and antinodes in the weld melt line such that, by comparing microstructure samples cut from both node and antinode regions, cavitation effects on weld quality improvement can be directly revealed.

Author Contributions: T.-H.G., P.C. and J.K. developed the concept for this study. Laboratory experiments and formal analysis were performed by A.T. and J.S; J.K.; Original draft was written by A.T. and J.S. and reviewed and edited by J.K and W.B.; T.-H.G., W.B. and P.C. were responsible for supervision, investigation and project administration; T.-H.G., P.C. and J.K. contributed to funding acquisition and to resources deployment. All authors have read and agreed to the published version of the manuscript.

Funding: This research was funded by Innovate UK grant number 102802. The APC was funded by Brunel University London.

Institutional Review Board Statement: Not applicable.

Informed Consent Statement: Not applicable.

Data Availability Statement: Not applicable.

Conflicts of Interest: The authors declare no conflict of interest.

References

1. Fathi, H.; Närhi, M.; Gumenyuk, R. Towards Ultimate High-Power Scaling: Coherent Beam Combining of Fiber Lasers. *Photonics* **2021**, *8*, 566. [CrossRef]
2. Katayama, S. *Handbook of Laser Welding Technologies*; Woodhead Publishing: Sawston, UK, 2013.
3. Teyeb, A.; Lowe, P.S.; Kanfoud, J.; Gan, T.H. Investigation of the use of power ultrasonic to improve the laser welding of Aluminium alloys. *Int. J. Mech. Prod. Eng.* **2018**, *6*, 51–54.
4. Oladimeji, O.; Taban, E. Trend and innovations in laser beam welding of wrought aluminium alloys. *Weld World* **2016**, *60*, 415–457. [CrossRef]
5. Gallego-Juárez, J.A.; Rodriguez, G.; Acosta, V.; Riera, E. Power ultrasonic transducers with extensive radiators for industrial processing. *Ultrason. Sonochem.* **2009**, *17*, 953–964. [CrossRef] [PubMed]
6. Hagenlocher, C.; Fetzer, F.; Weller, D.; Weber, R.; Graf, T. Explicit analytical expressions for the influence of welding parameters on the grain structure of laser beam welds in aluminium alloys. *Mater. Des.* **2019**, *174*, 107791. [CrossRef]
7. Eskin, D.G. Ultrasonic processing of molten and solidifying aluminium alloys: Overview and outlook. *Mater. Sci. Technol.* **2016**, *33*, 636–645. [CrossRef]
8. Dubey, A.K.; Yadava, V. Laser beam machining—A review. *Int. J. Mach. Tools Manuf.* **2008**, *48*, 609–628. [CrossRef]
9. Silva, J. Laser Welding of Aluminium Rings. Mastery Thesis, Instituto Superior Técnico, Universidade Técnica de Lisboa, Lisboa, Portugal, 2011.
10. Todaro, C.J.; Easton, M.A.; Qiu, D.; Zhang, D.; Bermingham, M.J.; Lui, E.W.; Brandt, M.; StJohn, D.H.; Qian, M. Grain structure control during metal 3D printing by high intensity ultrasound. *Nat. Commun.* **2020**, *11*, 142. [CrossRef] [PubMed]
11. Cochrane, R.F.; Dalgarno, K.W. Review on selective laser sintering/melting (SLS/SLM) of aluminium alloy powders: Processing, microstructure, and properties. *Prog. Mater. Sci.* **2015**, *74*, 401–477.
12. Krajewski, W.; Wlosinski, T.; Chmielewski, I.; Kolodziejczak, P. Ultrasonic-vibration assisted arc-welding of aluminum alloys. *Bull. Pol. Acad. Sci. Tech. Sci.* **2012**, *60*, 841–852. [CrossRef]
13. Kumar, S.; Wu, C.S.; Padhy, G.K.; Ding, W. Application of ultrasonic vibrations in welding and metal processing: A status review. *J. Manuf. Process.* **2017**, *26*, 295–322. [CrossRef]
14. Puga, H.; Costa, S.; Barbosa, J.; Ribeiro, S.; Prokic, M. Influence of ultrasonic melt treatment on microstructure and mechanical properties of AlSi9Cu3 alloy. *J. Mater. Process. Technol.* **2011**, *211*, 1729–1735. [CrossRef]
15. Leong, T.S.; Martin, G.J.; Ashokkumar, M. Ultrasonic encapsulation—A review. *Ultrason. Sonochem.* **2016**, *35*, 605–614. [CrossRef]
16. Bakhtiyari, A.N.; Wang, Z.; Wang, L.; Zheng, H. A review on applications of artificial intelligence in modeling and optimization of laser beam machining. *Opt. Laser Technol.* **2021**, *135*, 106721.
17. Yuan, D.; Shao, S.; Guo, C.; Jiang, F.; Wang, J. Refining of Ti-6Al-4V alloy fabricated by laser and wire additive manufacturing assisted with ultrasonic vibration. *Ultrason. Sonochem.* **2021**, *73*, 105472. [CrossRef]
18. Franco, E.E.; Meza, J.M.; Buiochi, F. Measurement of elastic properties of materials by the ultrasonic through-transmission technique. *Dyna* **2011**, *78*, 58–64.
19. Available online: Http://www.sonicsystems.co.uk/userfiles/downloads/9/P100-20%20Equipment%20Specification.pdf (accessed on 10 January 2022).
20. Leitner, M.; Leitner, T.; Schmon, A.; Aziz, K.; Pottlacher, G. Thermophysical Properties of Liquid Aluminum. *Metall. Mater. Trans. A* **2017**, *48*, 3036–3045. [CrossRef]
21. Jeong, I.L.; Jung, K.J.; Lee, K.; Kim, J.; Hoon, C.H.O. Experiment and Modeling to Assess Ultrasonic Attenuation Factor in Molten Aluminum Alloy. In Proceedings of the Symposium on Ultrasonic Electronics, Pukyong National University, Busan, South Korea, 16–18 November 2016; Volume 37.